www.sciencetranslationalmedicine.org/cgi/content/full/7/302/302ra134/DC1

Supplementary Materials for

Pronounced species divergence in corticospinal tract reorganization and functional recovery after lateralized spinal cord injury favors primates

Lucia Friedli, Ephron S. Rosenzweig, Quentin Barraud, Martin Schubert, Nadia Dominici, Lea Awai, Jessica L. Nielson, Pavel Musienko, Yvette Nout-Lomas, Hui Zhong, Sharon Zdunowski, Roland R. Roy, Sarah C. Strand, Rubia van den Brand, Leif A. Havton, Michael S. Beattie, Jacqueline C. Bresnahan, Erwan Bézard, Jocelyne Bloch, V. Reggie Edgerton, Adam R. Ferguson, Armin Curt, Mark H. Tuszynski, Grégoire Courtine*

*Corresponding author. E-mail: gregoire.courtine@epfl.ch

Published 26 August 2015, *Sci. Transl. Med.* **7**, 302ra134 (2015)
DOI: 10.1126/scitranslmed.aac5811

This PDF file includes:

Materials and Methods
Fig. S1. Clinical cases and experimental models of Brown-Séquard syndrome.
Fig. S2. Kinematics analysis uncovers similar patterns of locomotor deficits and compensation across species.
Fig. S3. Humans and monkeys, but not rats, recover hand kinematics and muscle activation patterns.
Fig. S4. Spinal cord decussating corticospinal fibers below the injury establishes synaptic contacts with neurons projecting to lumbar segments in monkeys.
Fig. S5. Increased density of corticospinal fibers above the hemisection in both rats and monkeys.
Fig. S6. Increased density of corticospinal tract fibers originating from the ipsilesional motor cortex fibers in segments below the hemisection in both rats and monkeys.
Fig. S7. Density of 5-hydroxytryptamine fibers below the hemisection remains unchanged in both monkeys and rats.
Fig. S8. The motor cortex fails to regain access to motoneurons below the hemisection in rats.
Table S1. Computed gait parameters.
Legends for movies S1 and S2

Other Supplementary Material for this manuscript includes the following:

(available at
www.sciencetranslationalmedicine.org/cgi/content/full/7/302/302ra134/DC1)

Movie S1 (.mp4 format). Recovery of locomotion in monkeys and humans compared to rats after a lateral hemisection of the spinal cord.
Movie S2 (.mp4 format). Recovery of hand function in monkeys and humans compared to rats after a lateral hemisection of the spinal cord.

MATERIALS AND METHODS

EMSCI database

Recovery of upper and lower limb function was analyzed in a total of 437 individuals who suffered a cervical SCI. All individuals were included in the EMSCI database (www.emsci.org). For each subject, we computed a laterality index that quantified the extent of asymmetry in functional deficits at 2 weeks post-SCI. This index was derived from the international standards for neurological classification of spinal cord injury (ISNCSCI), which combine both sensory (pinprick and touch) and motoric (motor score) evaluations. Pinprick scores, which primarily evaluate the integrity of the spinally decussating spinothalamic tract, contributed to the contralateral sensory score. Motor scores were calculated for each limb and side as the combined ASIA motor scores of all the segments below the lesion. The segments C2 to T1 contributed to upper limb motor scores, while segments T2 and below contributed to lower limb motor scores. Sensory and motor scores were summed to generate a sensorimotor score for each limb and side. The laterality index was computed as the difference between left and right sensorimotor scores divided by their sum. Consequently, a value equal to 0 would correspond to perfectly symmetrical deficits and a value equal to 1 would correspond to a pure Brown-Séquard syndrome. Functional recovery was computed as the relative increase in sensorimotor scores for each limb and side at 6 or 12 months compared to evaluations carried out at 2 weeks post-SCI.

EMSCI institutional members

Initiator and leading center

· Uniklinik Balgrist, Zentrum für Paraplegie, Zürich (Switzerland)

Founding members

· Klinik für Paraplegiologie, Universitätsklinikum Heidelberg, Heidelberg (Germany)

· Klinikum Bayreuth, Bayreuth (Germany)

· UMC St. Radboud, Nijmegen (The Netherlands)

Active members

- RKU - Universitäts- und Rehabilitationskliniken Ulm, Ulm (Germany)
- BG Kliniken Bergmannstrost Halle, Halle (Germany)
- Institut Guttmann, Barcelona (Spain)
- SRH Klinikum Karlsbad-Langensteinbach, Karlsbad (Germany)
- BG Unfallklinik Murnau, Murnau (Germany)
- Werner-Wicker-Klinik, Bad Wildungen (Germany)
- Motol Hospital, Prague (Czech Republic)
- Orthopädische Klinik Hessisch Lichtenau, Hessisch-Lichtenau (Germany)
- Hospital Nacional de Parapléjicos, Toledo (Spain)
- Schweizer Paraplegiker-Zentrum, Nottwil (Switzerland)
- The Queen Elizabeth National Spinal Injury Unit, Glasgow (Scotland)
- Ospedale Fondazione Santa Lucia, Rome (Italy)

Passive members

- BG Universitätsklinikum Bergmannsheil, Bochum (Germany)
- Clinique romande de réadaptation, Sion (Switzerland)
- BG Unfallklinik Tübingen, Tübingen (Germany)
- BG Unfallklinik Frankfurt am Main, Frankfurt a.M. (Germany)
- BG Unfallkrankenhaus Hamburg, Hamburg (Germany)
- Hôpital Raymond-Poincaré, Garches/Paris (France) (Founding Member)

Associated members

- Charité, Department of Experimental Neurology, Berlin (Germany)
- ICORD (International Collaboration on Repair Discoveries), Vancouver (Canada)

EMG electrodes

All surgical procedures used have been described previously (*5*). Under aseptic conditions and general anesthesia (1-2.5% Attane Isoflurane, Piramal Healthcare Limited, Mumbai, India), both rats and monkeys were implanted with bipolar intramuscular EMG electrodes (AS632, Cooner Wire) into selected hindlimb and forelimb muscles. In subsets of rats and monkeys, the following muscles were implanted: soleus and tibialis anterior for both hindlimbs; the biceps brachii, triceps brachii, extensor digitorum communis and flexor digitorum profundis of the ipsilesional forelimb. The ipsilesional flexor pollicis brevis also was implanted in monkeys. The proper location of EMG electrodes was verified post-mortem. The electrodes were connected to a head-mounted connector in rats, and an implanted telemetry recording system in monkeys (Konigsberg Instruments). Analgesia and antibiotics were provided post-surgically under monitoring of certified veterinaries.

After completion of pre-injury recordings, a second surgery was performed. A partial laminectomy followed by a lateral hemisection was made at the C7 spinal segment. In both rats and monkeys, a surgical micro-knife was mounted on a stereotaxic arm, positioned at the spinal midline and midway between the C5 and C6 dorsal laminae. This rostrocaudal position corresponds to the C7 spinal segment, as previously described (*5*). A micro-scissor was used several times to cut all the entire grey and white matters lateral to the inserted micro-knife. Two monkeys received the lateral hemisection using the same technique but at T10 spinal segment. The segment containing the lesion was reconstructed by a continuous series of Nissl stained sections. The lesion area was delimited for each section, and the area of maximum damage projected into a plane to obtain a lesion reconstruction (fig. S1, D and E).

Cortical electrodes

A subset of rats (n = 8) was implanted with an epidural monopolar electrode over the hindlimb area of the contralesional motor cortex to deliver stimulation. A reference electrode was positioned near the shoulder girdle (*13*).

Gait data analysis

For the ladder, 20-step cycles were extracted for analysis. Additional parameters related to the positioning of the foot (or paw) with respect to the successive rungs of the ladder were calculated to assess the precision of foot (or paw) placement during gait. A PC analysis was applied on all computed parameters with two objectives: (i) to assess the degree of locomotor recovery compared to pre-lesion or healthy subjects, and (ii) to extract, for each limb and species, the most relevant parameters to account for lesion-induced changes in ipsilesional and contralesional leg movements. For each species, all computed parameters were mean-centered and variance-scaled to obtain dimensionless values ranging from -1 to 1. PC analysis was applied on the normalized parameters for each species and for all species combined. Average scores for each limb and condition were extracted and the relative degree of functional recovery was measured as the 3-D distance between pre- and post-lesion (early and chronic) data points in the space created by PC1-3. Parameters with high factor loadings (|value| > 0.5) on PC1 and PC2 were extracted and regrouped into functional clusters.

Kinetmatics and electomyographic recordings

Reflective markers were attached to the shaved skin of rats and humans overlying leg or arm landmarks for locomotion and hand function assessment, respectively. Reflective painting was used for monkeys. The landmarks for the legs were the iliac crest, greater trochanter, knee joint, malleolus, fifth metatarsal, and outside tip of the fifth or fourth digit. The landmarks for the arm were the anterior border of the scapula, head of the humerus, elbow joint, distal head of the ulna, metacarpo-phalangeal joint, and outside tip of the third digit. The body was modeled as an interconnected chain of rigid segments, and joint angles were generated accordingly. In humans, bipolar surface electrodes (1 cm diameter, electrode separation of 1 cm) connected to a wireless transmitter (Myon) were placed over leg (medial gastrocnemius, soleus, tibialis anterior) and arm (biceps brachii, triceps brachii, extensor digitorum communis and flexor digitorum superficialis) muscles during locomotor and hand function assessments, respectively. A ground electrode was placed on the wrist. In all the species, signals were sampled at 2 kHz, amplified, band-pass filtered (10-1000 Hz), stored, and synchronized on-line (Vicon Nexus) or off-line (SIMI) for kinematics analysis.

Anterograde tracing

Rats and monkeys underwent anterograde tracing of corticospinal projections from both left and right motor cortex using tracers. All animals were anesthetized deeply as described above. In monkeys biotinylated dextran amine (BDA; 10% solution in water; 10,000 Da; Molecular Probes) was injected at 150 nl/site into 127 sites spanning the arm, trunk, and leg regions of the right motor cortex. Dextran-conjugated Alexa488 (D-A488) was injected using the same methods into the corresponding coordinates in the left motor cortex. The two monkeys with thoracic hemisection also received unilateral infusion of the retrograde tract tracing Fastblue (2% in 0.1-M phosphate buffer and 2% DMSO, EMS-CHEMIE) into the L2-L3 spinal segments. A total of 2.1 µl was pressure-injected over 7 sites (depth, 4.0 mm; space between injections, 1 mm). Seven weeks later, the monkeys were anesthetized deeply and perfused transcardially with a 4% solution of paraformaldehyde.

For rats, BDA (10% solution in H_2O; 10,000 molecular weight) was injected at 500 nl /site into 10 sites spanning the forelimb, trunk, and hindlimb regions of the right or left motor cortex. Three weeks later, rats were anesthetized by an intraperitoneal injection of 0.5 ml sodium pentobarbital (50 mg/ml) and perfused transcardially with approximately 80 ml Ringer's solution containing 100,000 IU/l heparin (Roche) and 0.25% $NaNO_2$ followed by 300 ml of cold 4% phosphate-buffered paraformaldehyde, pH 7.4, containing 5% sucrose.

Our standard protocols were used to detect traced corticospinal fibers and 5-HT fibers using goat anti-5-HT antibodies for monkeys (Immunostar; 1:10,000 in TBS-X) and rabbit anti-5-HT antibodies for rats (Sigma Aldrich; 1:5000 in blocking solution containing 4% NGS) (*13*). Traced corticospinal fibers were co-labeled with the synaptic protein synaptophysin using mouse anti-synaptophysin antibodies (Millipore; 1:1000 in blocking solution containing 4% NGS) or the vesicular transporter of glutamate (vGlut1) using guinea pig anti-vGlut1 antibodies (Millipore; 1:2000 in blocking solution containing 2% NGS).

Tissue processing

The spinal cord dura was removed and the spinal cord was cut in the transverse plane into blocks, using the nerve roots as a guide for the spinal levels. The block containing the lesion was sectioned in the horizontal plane on a freezing microtome or a cryostat set at 30 µm intervals. Analogous blocks were obtained from the intact animals. Blocks containing segments C3-C6 and

C8-T2 were sectioned in the transverse plane on a freezing microtome or a cryostat set at 40 µm. Cut tissue sections were stored at -20°C for monkeys and at 4°C for rats in cryoprotectant (25% glycerin, 30% ethylene glycol in 0.5 M phosphate buffer). Lesion extent was assessed using a 30-µm-thick horizontal section stained for Nissl substance. Transverse sections from the tissue blocks immediately rostral and caudal to the lesion block (segments C3-C4 and C8-T1) were selected for analysis of corticospinal tract and 5-HT fiber density. Our standard protocols were used to detect traced corticospinal fibers (*5, 13*) and 5-HT fibers using goat anti-5-HT antibodies for monkeys (Immunostar; 1:10,000 in TBS-X) and rabbit anti-5-HT antibodies for rats (Sigma Aldrich; 1:5000 in blocking solution containing 4% NGS).

Quantification of fiber density and axons

The capture and adjustment of anatomical images for quantification were performed as described previously (*5, 13*). For corticospinal fiber density quantification of 3 sections for monkeys and 5 sections for rats were randomly selected per animal. The fiber density of the gray matter for each animal was obtained using confocal stacks acquired with standard imaging settings and analyzed using custom-written Matlab (MathWorks) scripts according to previously described methods (*13*). Additionally, the number of labeled axons crossing the spinal cord midline was counted manually in each section used for the fiber density analysis. For 5-HT quantification of monkey sections, Stereo Investigator was used to outline lateral motor pools under low magnification and generate optical fractionator sampling sites. With a 100x objective, intersections of 5-HT-labeled axons with the inclusion lines of these sampling sites were marked. For rats, the same regions were quantified using the same methods as described for corticospinal tract axons. Serial reconstructions of some CST axons were performed as described previously for both monkey and rat sections below the level of injury (*5, 13*). An investigator who was blind to experimental conditions performed all tissue evaluations.

Syndromic analysis

To evaluate the effect of species on the integrated syndromic outcome after SCI (*7*), we used non-linear principal components analysis (NLPCA). This method uses a combination of optimal scaling and variance-maximization procedures to detect coherent patterns in data involving linear or non-linear relationships and across metrics with diverse scaling (categorical, ordinal, numeric)

(*15*). We performed separate NLPCA extractions for rat-monkey and rat-human data using variable subsets that allowed direct cross-species comparisons. Datasets from kinematics, food-retrieval success, and anatomical measures were manually curated and combined into a single large dataset for monkeys and rats. Treadmill and ladder locomotion kinematics and neurophysiological measures were combined from human and rat data. Bivariate correlation matrices were created for each combination of outcomes. Syndromic analysis was performed in SPSS Categories v. 19 to generate syndromic variables (PC1-2) specific to either rat-monkey or rat-human comparisons. PC1 is the shared variance (%) of all measures as they move together in a multivariate space with each measure loading (weighted arrows) onto PC1 based on their respective correlation to the entire syndrome (Fig. 7, B and C).

SUPPLEMENTARY FIGURES

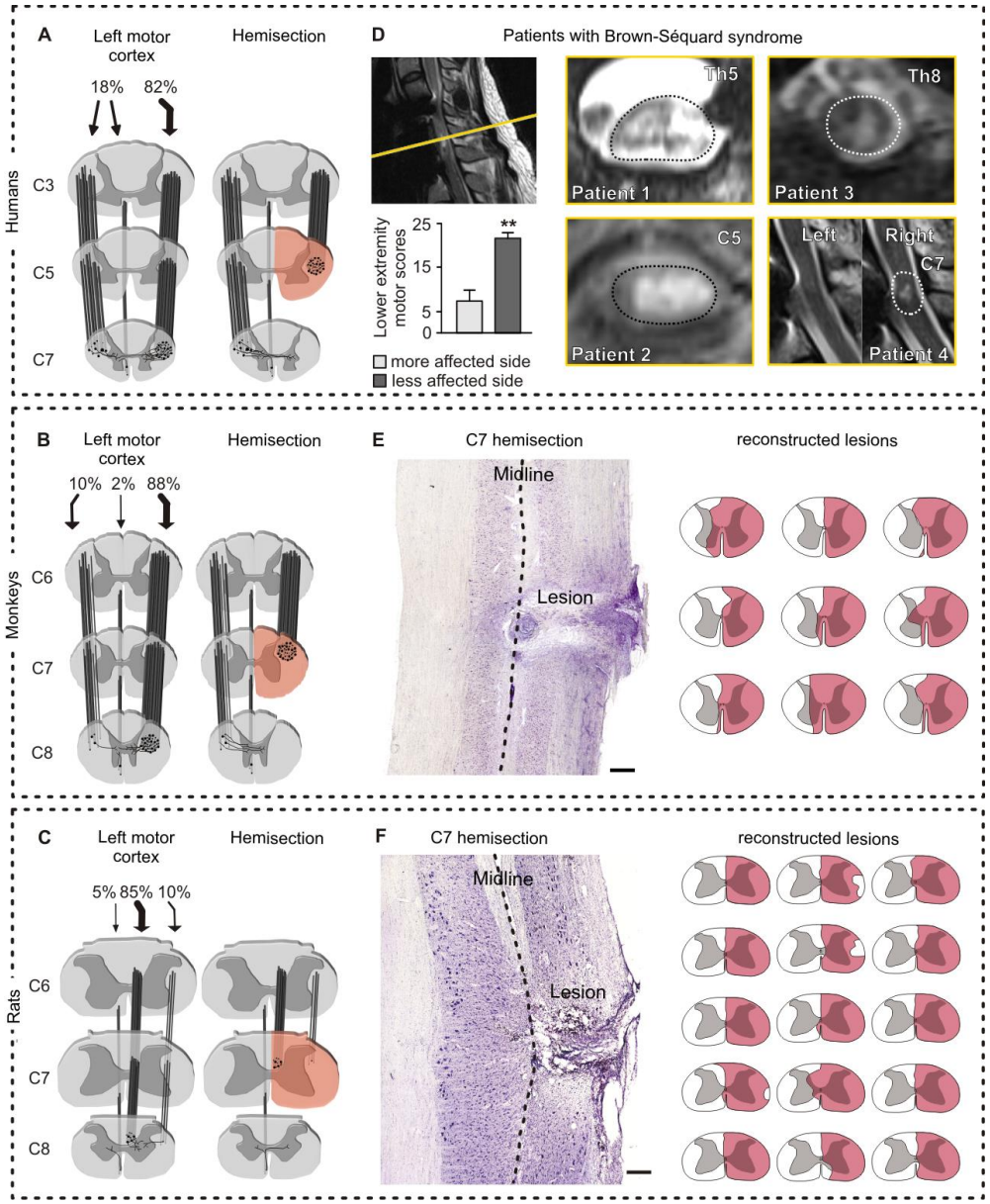

Figure S1: Clinical cases and experimental models of Brown-Séquard syndrome. (**A** to **C**) Schematic representation of corticospinal axonal projections in the spinal cord white and grey matter of humans, monkeys, and rats, respectively, before injury (healthy) and after a lateral hemisection. (**D**) MR images through the transverse plane obtained in the 4 SCI patients who participated in the longitudinal study. The level of the lesion is indicated in each MRI. Histograms show the mean values (± SEM) of lower extremity scores at early time-points after the lesion (n = 4) $^{**}P < 0.01$, Friedman test. (**E** and **F**) Representative Nissl staining of a longitudinal section of the hemisected spinal cord in rats and monkeys. For each animal, the extent of the injured area was measured using camera lucida reconstructions. The surface of maximal damage per quarter of spinal cord was calculated to generate a measure of spared tissue. Scale bars: 1 mm for monkeys, 300 µm for rats.

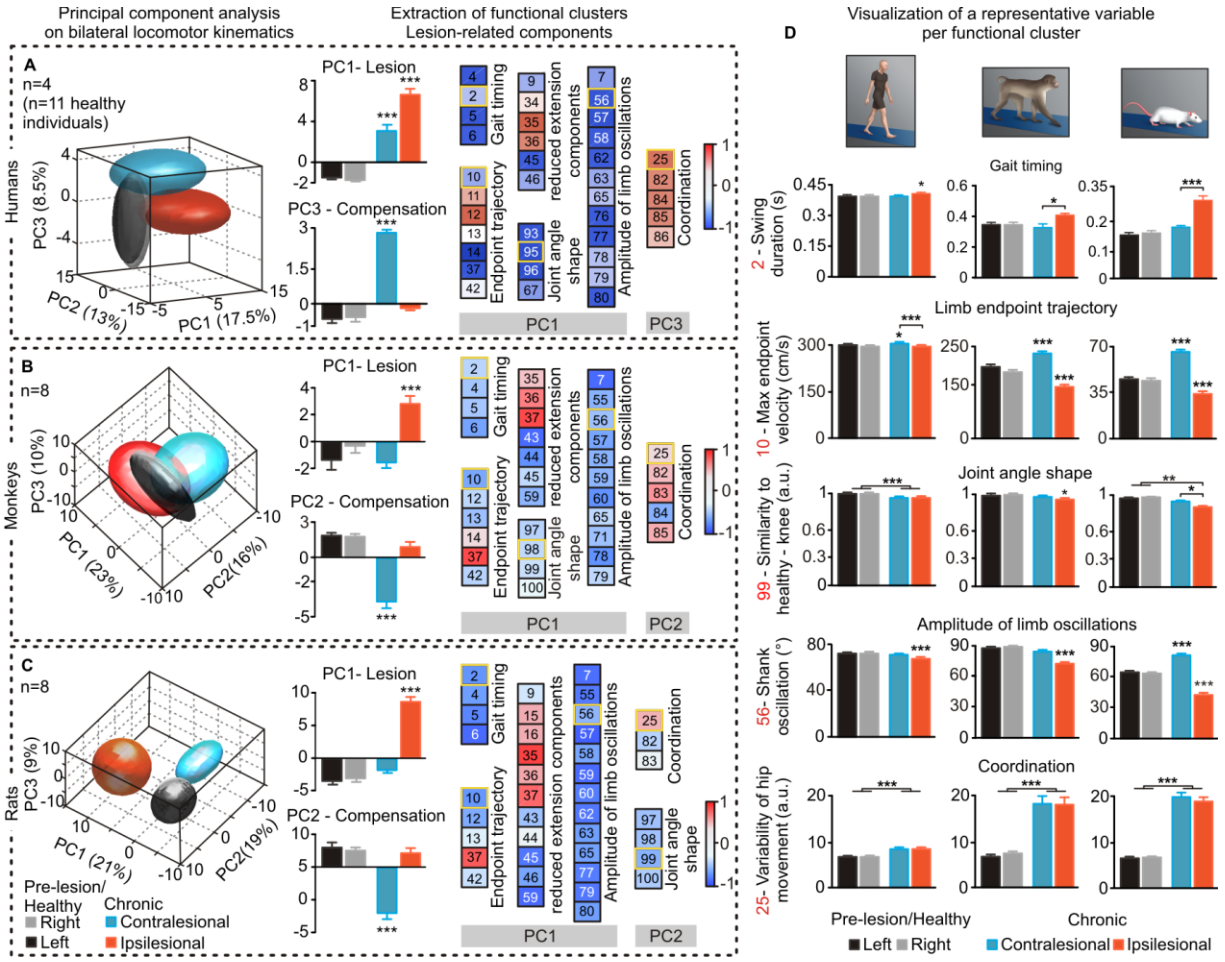

Figure S2: Kinematics analysis uncovers similar patterns of locomotor deficits and compensation across species. (**A** to **C**) PC analysis was applied on all the gait parameters measured for the left and right legs before the injury (or healthy), and at the chronic stage of the SCI. Gait clusters related to the left and right legs co-localized in non-injured humans (A), monkeys (B), and rats (C). In the chronic stage, gait clusters corresponding to the contralesional and ipsilesional legs moved in opposite directions, indicating side-specific alteration of gait patterns. Histograms show the mean values of scores for the left and right legs before the injury (or healthy) and at the chronic stage of the lesion. For each species, PC1 and PC2 distinguished the ipsilesional and contralesional legs, respectively. Correlations between parameters and PC1 and PC2, termed factor loadings, were extracted and regrouped into functional clusters that we named for clarity. The numbers refer to individual parameters that were calculated with the exact same methods in humans, monkeys, and rats (table S1). The same list of parameters loaded on PC1 and PC2 in humans, monkeys, and rats indicate that a lateral hemisection SCI induces similar deficits and compensation in all the studied species. (**D**) Gait parameters using more conventional representations: mean values of parameters with high factor loadings on PC1, which are framed in yellow in the functional clusters. **P* < 0.05, ***P* < 0.01, ****P* < 0.001, ANOVA. Data are means ± s.e.m. (*n* indicated in figure)

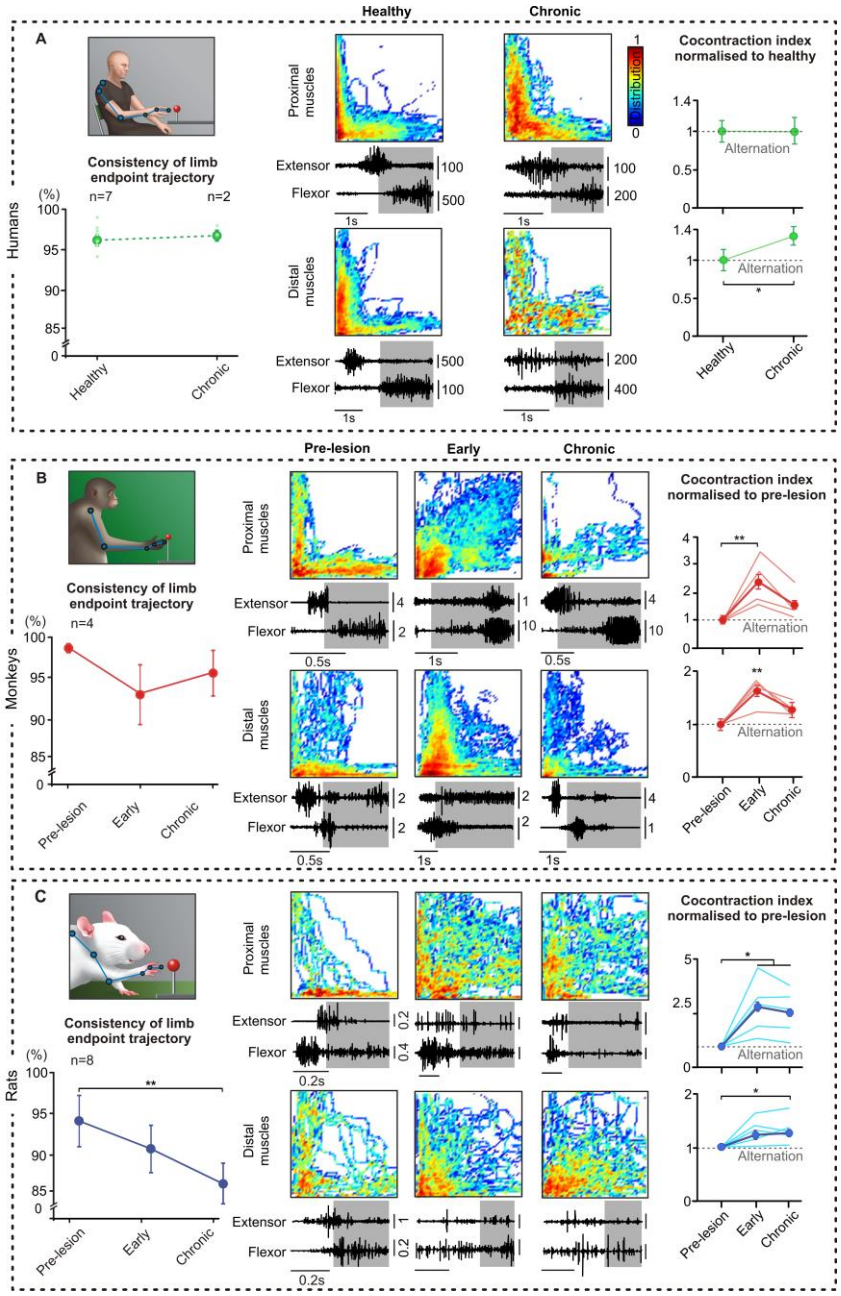

Figure S3: Humans and monkeys, but not rats, recover hand kinematics and muscle activation patterns. (A to **C)** The consistency of reaching movements was measured as the percent of explained variance by PC1 when applying a PC analysis on 10 successive 3D reaching trajectories. Representative examples of the recruitment pattern for proximal and distal pairs of antagonist muscles are shown during a reach and grasp. The empty and shaded areas correspond to the reach and grasp phases, respectively. The color-coded plots show, for each pair of antagonistic muscles, the probability of co-activation. An L-shaped pattern indicates reciprocal activation between antagonist muscles, while a filled pattern highlights a high degree of co-activation. Line plots showing the normalized values of the co-contraction index computed for proximal and distal antagonistic muscle pairs before the SCI (or healthy) and at the chronic stage. Thin lines correspond to individual data. **P* < 0.05, ***P* < 0.01, ANOVA. Data are means ± s.e.m. (*n* indicated in figure).

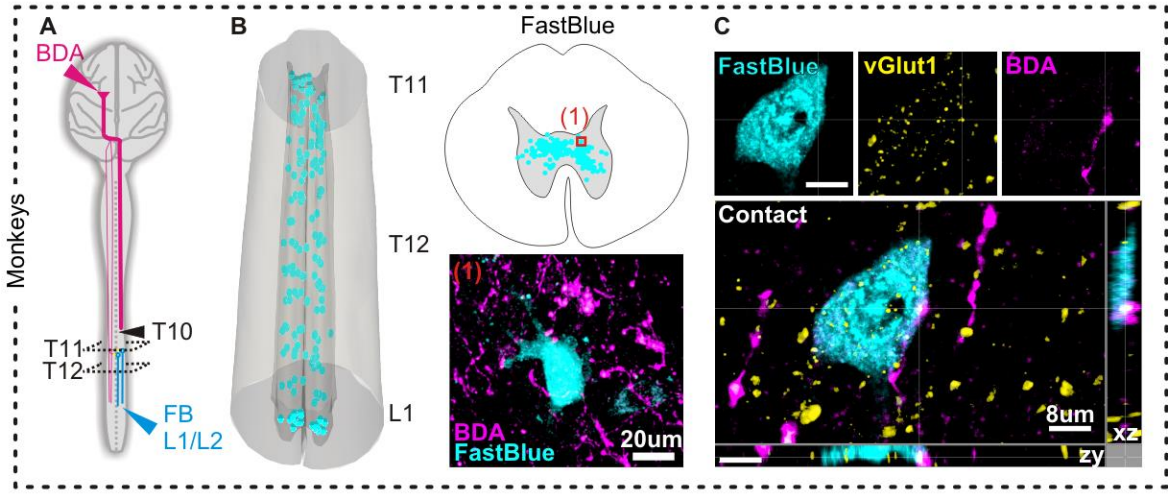

Figure S4: Spinal cord decussating corticospinal fibers below the injury establishes synaptic contacts with neurons projecting to lumbar segments in monkeys. (**A**) Diagram illustrating the anatomical experiments and analyzed regions. (**B**) Reconstruction of neurons retrogradelly labeled from L1/L2 segments and a representative image of corticospinal fibers surrounding one of these neurons. The image was taken from the intermediate laminae of the T12 spinal segment, on the side of the hemisection. (**C**) Representative images (*n* = 2 monkeys) showing 3D co-localization of BDA and vGlut1 synaptic terminals in close apposition to a neuron retrogradelly labeled from L1/L2, which demonstrate the presence of synaptic terminals onto sub-lesional corticospinal fibers that contact intraspinal neurons.

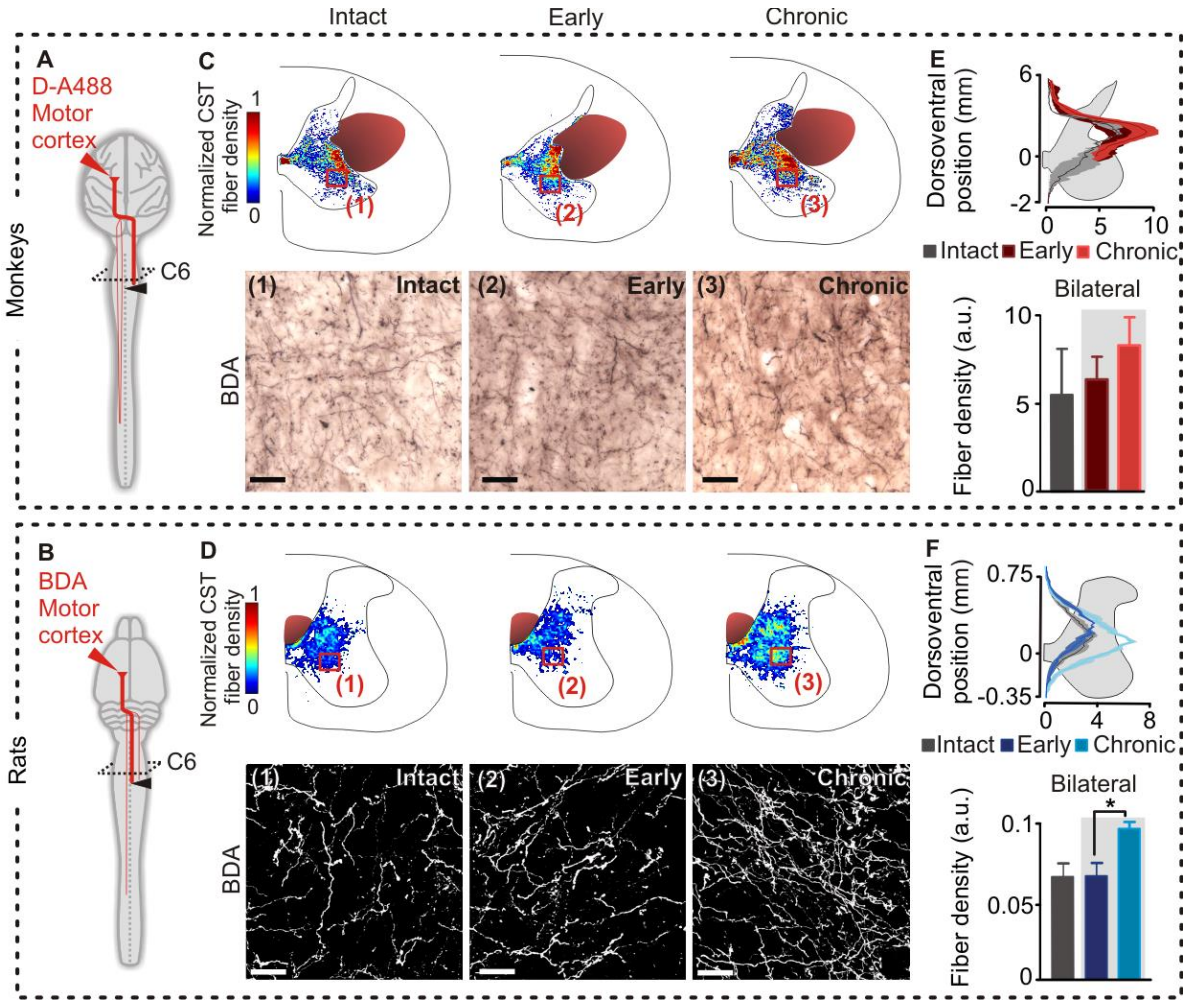

Figure S5: Increased density of corticospinal fibers above the hemisection in both rats and monkeys. (**A** and **B**) Diagrams illustrating the anatomical experiments and analyzed regions in monkeys and rats. (**C** and **D**) Heat maps of corticospinal tract fiber density in the ipsilesional C6 segment, together with representative photographs of corticospinal tract fibers from indicated regions in monkeys and rats. Scale bars, 100 and 30 μm for monkeys and rats, respectively. (**E** and **F**) Corticospinal tract fiber density distribution and the averaged density of corticospinal tract fibers in the analyzed C6 segment. **P* < 0.05, ANOVA. Data are means ± s.e.m. (*n* = 7 monkeys, *n* = 7 rats for chronic subjects; *n* = 3 monkeys, *n* = 8 rats for early subjects).

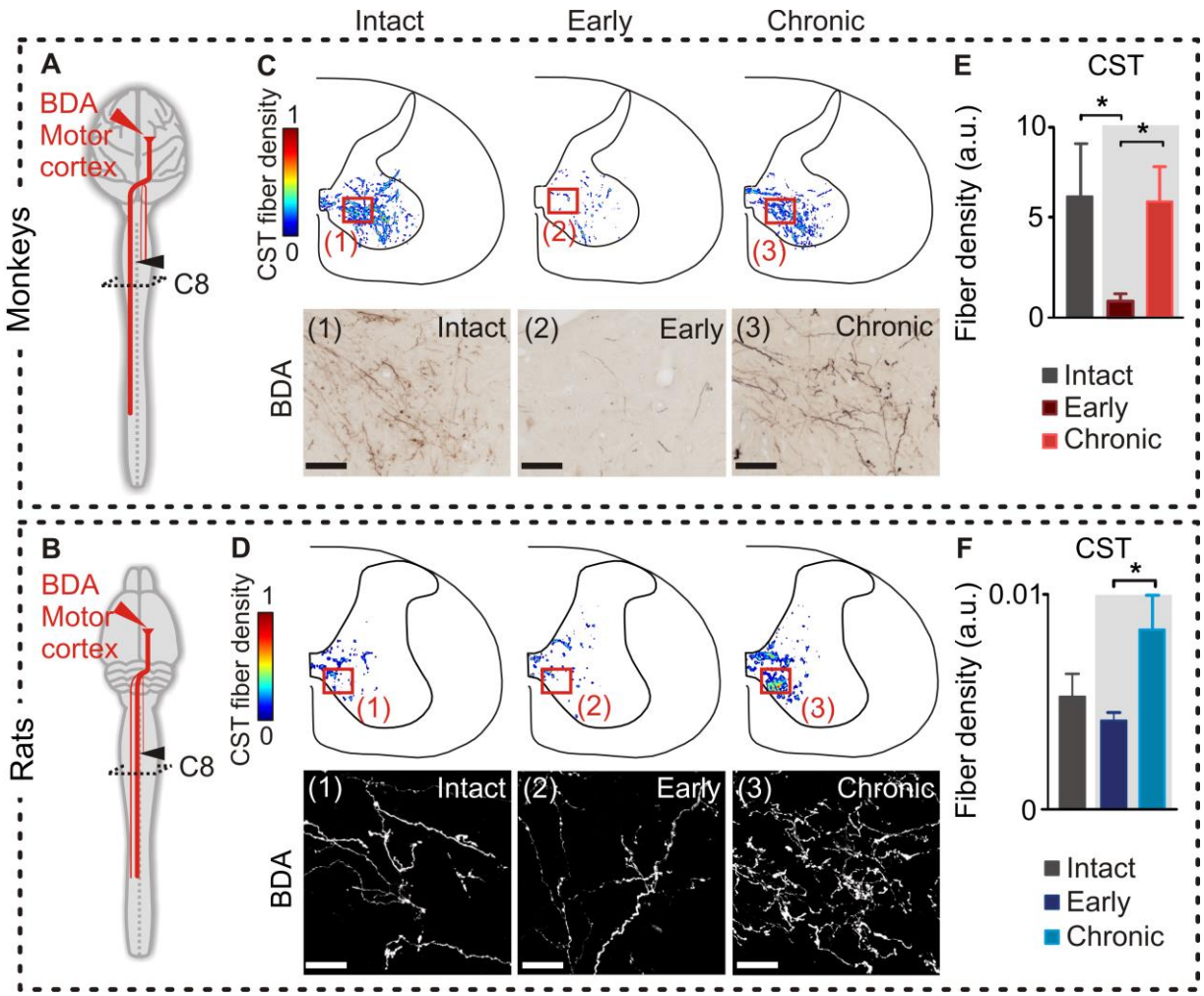

Figure S6: Increased density of corticospinal tract fibers originating from the ipsilesional motor cortex fibers in segments below the hemisection in both rats and monkeys. (A and **B)** Diagrams illustrating the anatomical experiments and analyzed regions in monkeys and rats. (**C** and **D**) Heat maps of corticospinal tract fiber density in the ipsilesional C8 segment, below the SCI, together with representative images of corticospinal tract fibers in monkeys and rats. Scale bars, 100 µm for monkeys and 30 µm for rats. (**E** and **F**) Average density (± SEM) of corticospinal tract fibers in the ipsilesional hemicord of the C8 segment. **P* < 0.05, ANOVA. Data are means ± s.e.m. (*n*= 7 monkeys, *n* = 5 rats for chronic subjects; *n* = 3 monkeys, *n* = 7 rats for early subjects).

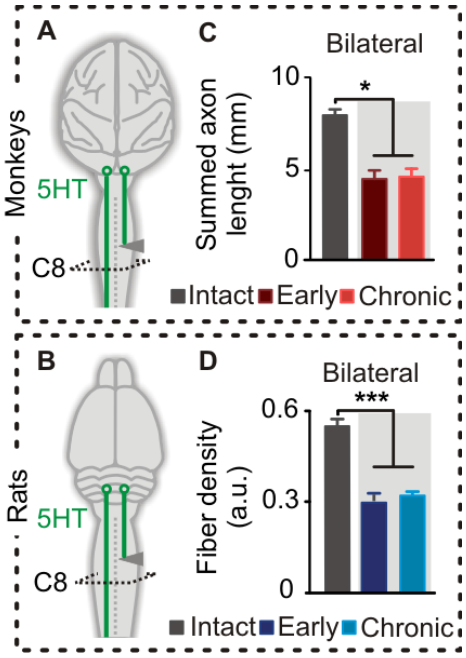

Figure S7: Density of 5-hydroxytryptamine fibers below the hemisection remains unchanged in both monkeys and rats. (**A** and **B**) Diagrams illustrating the anatomical experiments and analyzed regions in monkeys and rats. (**C** and **D**) Average density of 5-HT fibers in the analyzed C8 segment, below the hemisection. **P* < 0.05, ****P* < 0.001, ANOVA. Data are means ± s.e.m. (*n* = 7 monkeys, *n* = 5 rats for chronic subjects; *n* = 3 monkeys, *n* = 8 rats for early subjects).

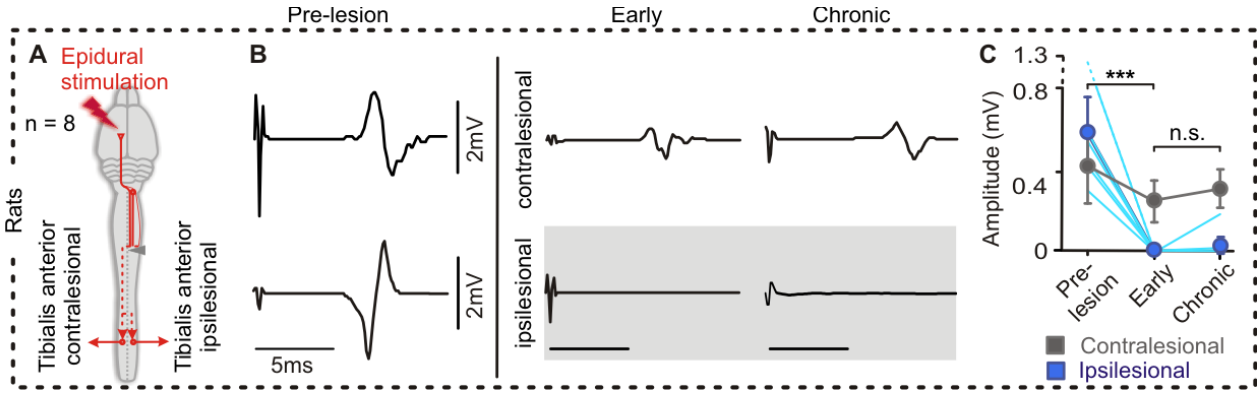

Figure S8: The motor cortex fails to regain access to motoneurons below the hemisection in rats. (**A**) Diagram illustrating the electrophysiological experiment including the stimulation and recording sites. All electrodes were implanted chronically. Stimulation was delivered under fully awake conditions, while the rat was standing quietly. (**B**) Motor responses were elicited by an electrical pulse (0.5 ms) delivered over the hindlimb area of the left motor cortex. Motor responses were recorded from left and right ankle flexor muscle before and at an early and chronic time-point after hemisection. (**C**) Mean values of motor response amplitudes recorded before, and at an early and chronic time-point after hemisection. Thin lines correspond to individual data. ***$P < 0.001$, n.s., not significant, repeated-measure ANOVA. Data are means ± s.e.m. ($n = 8$ rats).

SUPPLEMENTARY TABLE

Table S1: Computed gait parameters. The various parameters computed from kinematic recordings. The numbers refer to the variables in PC analysis.

#	Computed parameters
	Gait timing
1	Stance duration
2	Swing duration
3	Relative stance duration (percent of the cycle duration)
	Fore- and hindlimb coordination
4	Correlation between whole hindlimb oscillations
5	Correlation between hindlimb and ipsilateral forelimb oscillations
6	Correlation between hindlimb and contralateral forelimb oscillations
	Limb endpoint (MTP) trajectory
7	Stride length
8	Step length
9	3D limb endpoint path length
10	Maximum backward position
11	Minimum forward position
12	Step height
13	Maximum speed during swing
14	Relative timing of maximum velocity during swing
15	Acceleration at swing onset
16	Endpoint velocity
17	Orientation of the velocity vector at swing onset
18	Dragging
19	Relative dragging duration (percent of swing duration)
	Stability
20	lateral movement of the foot during swing
21	Stance width
22	Maximum trunk vertical position
23	Minimal trunk vertical position
24	Amplitude of the vertical trunk position
25	Variability of sagittal trunk oscillations
26	Variability in velocity of sagittal trunk oscillations
27	Variability of Medio-lateral hip oscillations
28	Variability of vertical mid-point hip oscillations
29	Variability of Medio-lateral shoulder oscillations
30	Variability of vertical mid-point shoulder oscillations
31	Variability of Medio-lateral shoulder rotations
32	Variability of Medio-lateral hip rotations
33	Lateral oscillation of the center of mass
34	Vertical oscillation of the center of mass
35	3D oscillation of the center of mass
	Joint angles and limb segment oscillations
36	Crest oscillations
37	Thigh oscillations
38	Shank oscillations
39	Foot oscillations
40	Toe oscillations
41	Whole limb oscillations
42	Crest oscillations
43	Thigh oscillations
44	Shank oscillations
45	Foot oscillations
46	Toe oscillations
47	Whole limb oscillations
48	Hip joint angle
49	Knee joint angle
50	Ankle joint angle
51	MTP joint angle

#	Computed parameters
	Joint angles and limb segment oscillations (continued)
52	Whole limb adduction
53	Foot adduction
54	Hip joint angle
55	Knee joint angle
56	Ankle joint angle
57	MTP joint angle
58	Whole limb abduction
59	Foot abduction
60	Crest oscillations
61	Thigh oscillations
62	Leg oscillations
63	Foot oscillations
64	Toe oscillations
65	Whole limb oscillations
66	Hip joint angle
67	Knee joint angle
68	Ankle joint angle
69	MTP joint angle
70	Whole limb medio-lateral oscillations
71	Foot abduction /adduction
	Velocity
72	Whole limb oscillation velocity
73	Hip joint angle velocity
74	Knee joint angle velocity
75	Ankle joint angle velocity
76	MTP joint angle velocity
77	Whole limb oscillation velocity
78	Hip joint angle velocity
79	Knee joint angle velocity
80	Ankle joint angle velocity
81	MTP joint angle velocity
82	Whole limb angle velocity
83	Hip joint angle velocity
84	Knee joint angle velocity
85	Ankle joint angle velocity
86	MTP joint angle velocity
	Inter-limb coordination
87	Degree of linear coupling between joint oscillations
88	Temporal coupling between crest and thigh oscillations
89	Temporal coupling between thigh and leg oscillations
90	Temporal coupling between leg and foot oscillations
91	Temporal coupling between foot and toe oscillations
92	Correlation between crest and tight oscillations
93	Correlation between tight and leg oscillations
94	Correlation between leg and foot oscillations
95	Correlation between foot and toe oscillations
96	Correlation between hip and knee oscillations
97	Correlation between knee and ankle oscillations
98	Correlation between ankle and MTP oscillations
	Similarity to healthy gait
99	Correlation between limb oscillation of healthy and pathological leg
100	Correlation between hip oscillation of healthy and pathological leg
101	Correlation between knee oscillation of healthy and pathological leg
102	Correlation between ankle oscillation of healthy and pathological leg
103	Correlation between MTP oscillation of healthy and pathological leg

SUPPLEMENTARY MOVIES

Movie S1. Recovery of locomotion in monkeys and humans compared to rats after a lateral hemisection of the spinal cord. This movie illustrates the recovery of basic and ladder locomotion after a lateral hemisection of the spinal cord in primates and rats.

Movie S2. Recovery of hand function in monkeys and humans compared to rats after a lateral hemisection of the spinal cord. This movie illustrates the recovery of manual skills after a lateral hemisection of the spinal cord in primates and rats.